# Did the 28 October 2003 solar flare accelerate protons to $\gtrsim$ 20 GeV? A study of the subsequent Forbush decrease with the GRAPES-3 tracking muon telescope

T. Nonaka, Y. Hayashi, N. Ito, S. Kawakami, T. Matsuyama, A. Oshima, H. Tanaka, and T. Yoshikoshi
*Graduate School of Science, Osaka City University, Osaka 558-8585, Japan*

S. K. Gupta,* A. Jain, S. Karthikeyan, P. K. Mohanty, S. D. Morris, B. S. Rao, K. C. Ravindran, K. Sivaprasad, B. V. Sreekantan, S. C. Tonwar, and K. Viswanathan
*Tata Institute of Fundamental Research, Homi Bhabha Road, Mumbai 400 005, India*

H. Kojima
*Nagoya Women's University, Nagoya 467-8610, Japan*

(Received 14 February 2005; revised manuscript received 10 April 2006; published 18 September 2006)

Solar flares accelerate charged particles through a variety of mechanisms, which may be constrained through observations at high energies ( $>10$ GeV). We report here a search for direct emission of protons of energy $\gtrsim 20$ GeV in association with an X17 class solar flare that occurred on 28 October 2003, using a large area tracking muon telescope of the GRAPES-3 experiment at Ooty. Some features of the telescope, including its novel capability of high sensitivity search for the directional enhancement of the solar protons are also described. A 99% C.L. upper limit on the flux of protons due to the solar flare has been placed at $1.4 \times 10^{-6}$ cm$^{-2}$ s$^{-1}$ sr$^{-1}$. A separate upper limit on the narrow solid angle flux of protons at $4 \times 10^{-6}$ cm$^{-2}$ s$^{-1}$ sr$^{-1}$ is also placed. Solar flares are also associated with coronal mass ejections, which propagate through the interplanetary space producing geomagnetic storms and Forbush decrease (Fd) events, upon their arrival at the Earth. New information on the structure and time evolution of the large Fd observed on 29 October 2003 by GRAPES-3 is presented. The onset of Fd in nine different solid angle bins ( $\sim 0.3$ sr) shows a remarkably similar behavior, with an evolution on a time scale of $\sim$1 h. A power law dependence of the magnitude of the Fd on the cutoff rigidity has been derived, using the data from tracking muon telescope, over a narrow range of cutoff rigidity 14.3–24.0 GV, which shows a spectral slope "$\gamma = 0.53 \pm 0.04$," in agreement with earlier measurements.

DOI: 10.1103/PhysRevD.74.052003 PACS numbers: 96.50.Vg, 96.50.S−, 96.60.qe

## I. INTRODUCTION

The Sun is the closest astrophysical source accelerating particles to GeV and possibly higher energies, yet there is very limited understanding of, and little consensus on, the sites and processes leading to the production and acceleration of energetic particles associated with the solar flare activity. Here, we report on the search for the emission of protons of $\gtrsim 20$ GeV during the active phase of the large X17 class solar flare that started at 09:51 UTC (coordinated universal time) on 28 October 2003, using a large area tracking muon telescope of the GRAPES-3 experiment. Protons were accelerated during the solar flare on 28 October 2003 around 11:10 UTC nearly 80 min after the detection of this flare in the x rays. This solar flare had occurred in the active sunspot region 10 486 in the east of the central meridian of the Sun [1].

An intriguing feature of the solar flare of 28 October 2003 has been that the earliest arriving particles were recorded by the neutron monitors (NMs) viewing the antisunward direction. Also the enhancement in the nucleon flux continued for a long duration of time ( $\sim 20$ h) until the fast moving (mean velocity $\sim 2200$ km/s) coronal mass ejection (CME) shock front arrived at the Earth. Two distinct components, namely, a prompt and a delayed one, were observed by the global network of Earth-based NMs [2]. Detailed modeling of charged particle propagation in the interplanetary medium permeated with magnetic fields to explain the delayed and the prompt components of the solar particles, observed by the worldwide network of a large number of NMs, has been attempted by Miroshnichenko and co-workers [3]. These authors have exploited the delays in the onset of the rate increases seen in the NMs to estimate that the path length of the relativistic protons from the Sun to the Earth to be $\sim$2.2 AU. This model implies that the acceleration of the protons in the flaring region is followed by their transport along a stretched magnetic field loop ( $\sim 2.2$ AU) to the Earth. During this period the Earth was located at the interface of the interplanetary CME and a corotating stream from the Sun. The direction of the loop from the antisunward direction was used to explain the direction of the radiation and the anisotropy seen in the NM data.

The onset of the Forbush decrease (Fd) started in the wake of a fast CME [4], on 29 October 2003 nearly 20 h after the start of the X17 class solar flare at 09:51 UTC on 28 October 2003. Concurrent observations of sub-GeV solar neutrons using several NMs and of solar $\gamma$ rays from INTEGRAL satellite have been made with good statistical significance. The correlation in the time profiles

*Electronic address: gupta@grapes.tifr.res.in

 

of the solar neutrons and the $\gamma$ rays is used to conclude that the solar neutrons and the $\gamma$ rays were produced at the same time [5].

The available data obtained so far have shown that the solar flares and CMEs are a complex combination of a variety of physical processes involving the reconnection of the solar magnetic field lines due to certain instabilities occurring in the chromospheric and coronal regions surrounding the Sun. In some cases, the solar flares are observed in association with the CMEs. However, no such association between these two phenomena is seen in a number of other instances. The relationship between the emission mechanisms responsible for the solar flares and CMEs is an area of active research and much debate (see Ref. [6] and references therein). Solar flares are among the most energetic events to occur in the solar system, releasing vast amounts of energy ( $\sim 10^{25}$ J) on relatively short time scales ( $\sim 10^{2}$ s). Solar flares give rise to the emission of a variety of radiation ranging from radio, microwave, optical, soft and hard x rays, and $\gamma$ rays of up to several MeV including the $\gamma$ ray lines due to nuclear deexcitation. Energetic solar particles contain electrons and ions which are accelerated in the solar flares [7].

Solar flares are classified into two broad categories, namely, ''gradual'' and ''impulsive'' flares. The gradual flares occur higher up in the corona and generally last for a longer duration of time and are also spread over a larger geographical region on the Sun. The gradual flares are also associated with coronal mass ejections and are accompanied with soft and hard x-ray emission. The ions accelerated in the gradual events display a composition which is rather similar to that of the coronal abundances. The impulsive flares on the other hand are believed to emanate from the regions closer to the Sun in the chromosphere and/or lower corona; the emission takes place for a shorter duration of time and over a relatively compact geographical region. The composition of the energetic ions in the impulsive events displays a very significant enhancement of the heavier nuclei as compared to the coronal abundances by an order of magnitude or more. In the case of helium, the ratio $^{3}\mathrm{He}/^{4}\mathrm{He}$ is observed to be $\sim 1$ as compared to the coronal value of $\sim 10^{-3}$ [7,8].

Based on the observations, it appears that the ions in the gradual events are accelerated by a CME driven shock front. The shock front itself may be formed as a result of the magnetic reconnection, induced due to some instability in the coronal region. In the case of the impulsive events, several processes have been proposed for the modeling of the turbulent acceleration of particles in the flare region. Stochastic acceleration involving interaction of the particles with plasma waves gives a reasonable fit to some of the features of the energy spectra and the abundance ratios for several ions in the impulsive solar flares [7,9]. However, some of the recent observations have shown that this canonical scenario of different acceleration mechanisms and characteristics for the impulsive and gradual flares is not always valid. It has been argued that the mechanism(s) responsible for impulsive events may also accelerate ions in some gradual events leading to a heavy ion rich impulsive composition in those cases [10]. Alternatively in some instances, shock acceleration could play a significant role in the acceleration of the particles in impulsive events. This hypothesis has been borne out by the observation of a CME in association with an impulsive flare on 1 May 2000 [11].

While the primary particles generated in a solar flare are charged, and are accelerated in the solar convection zones which serve to transfer energy to the interaction regions in the chromosphere, the $\gamma$ ray and neutron emission provides information on the interaction between solar energetic particles and the ambient medium around the Sun. For example, the temporal profiles of the $\gamma$ ray flux at different energies provide a wealth of data on the interaction of various particles and their entrapment near the Sun. The continuum $\gamma$ ray emission is produced due to the bremsstrahlung from high energy electrons. The bombardment of the chromosphere by high energy ions leads to the excitation of the ambient matter resulting in the emission of $\gamma$ ray lines in the MeV region due to the nuclear deexcitation in the chromosphere [12]. On the other hand, solar neutrons provide crucial information on the interaction of energetic ions, as the neutrons escaping into the interplanetary medium can be observed as decay protons or electrons by the detectors in space, and in rare cases, through the recoil protons in the ground-based NMs. However, the NMs mostly observe secondary neutrons produced by the interaction of primary protons with air nuclei.

In terms of the requirement for the energy budget, the conversion of the magnetic potential energy into other forms, during the process of magnetic reconnection [13] provides a viable and attractive possibility to accelerate particles to several tens of GeV in a relatively short time. Therefore, there is a great deal of interest in exploring the energy spectrum of the particles emitted during the solar flares, over a broad range of energy. This becomes especially important in view of the fact that the NMs operating at high rigidities have only rarely recorded high energy events above 10 GeV. As in the other branches of astrophysics, a significant advance in the understanding of the phenomenon of the solar flares is unlikely to occur in the absence of multiwavelength observations with a variety of ground- and space-based instruments. This approach has been successfully employed in the case of the large solar flare that had occurred on 29 September 1989 [12].

While the satellite-borne detectors with high sensitivity such as the instruments aboard the Advanced Composition Explorer [14] provide excellent measurements at sub-GeV energies, the energy range spanning from a few GeV to tens of GeV, can only be explored through the studies, with the network of NMs and muon telescopes located at various sites around the world. The highest energy of the

particles accelerated during the solar flares is one of the decisive parameters that can be used to differentiate among various possible models of particle acceleration in the Sun. Observations of flare particles show spectra with cutoff at energies beyond a few GeV which have to be understood on the basis of the models of particle acceleration. Observations carried out using the detectors with high sensitivity opens up the possibility of search for particle fluxes at high energies near the cutoff and/or the shape of the energy spectrum near such cutoffs. Such measurements may provide new constraints on models of particle acceleration in solar flares. However, the galactic cosmic rays constitute the dominant background for the detection of the high energy (above tens of GeV) solar particles. The detection of the secondary muons (produced in the atmosphere by energetic solar particles) with the surface and the underground muon telescopes with good directional capability is an important tool to probe the high energy end point of the energetic solar particle spectrum. It has been pointed out that muon detectors with relatively good angular resolution may be able to observe the energetic solar particles at $\sim$100 GeV.

In the past, there have been several reports of the detection of the bursts of muons which were nearly coincident in time with the associated solar flare activity in x rays, although with somewhat limited statistical significance (see [12] and the references therein). One of the significant detection of a muon burst was by the Baksan group which occurred on 29 September 1989 at an energy of $\gtrsim$ 200 GeV, indicating possible acceleration of the solar protons to several hundreds of GeV. However, the direction of this muon burst did not coincide with the direction of the Sun. Also the enhanced muon flux was observed after a delay of a couple of hours after the impulsive phase of the associated solar flare [15]. The delayed arrival of the high energy solar particles opens up the possibility, in at least some of the solar flares, of the acceleration of high energy protons and ions after a significant delay, following the initial impulsive phase. The AGASA group had reported the detection of an enhanced flux of prompt muons during the solar flare of 4 June 1991, which they claimed was due to the arrival of the solar neutrons of energy $\geq$ 10 GeV [16]. The L3 group, using their precision tracking muon detectors at CERN, have reported the detection of a significant excess of muons in association with the solar flare of 14 July 2000 [17].

The occurrence of the solar flares and the CMEs result in a sudden injection of high energy plasma with frozen-in magnetic field lines into the interplanetary space. This phenomenon leads to the formation of a shock front in the interplanetary space surrounding the Sun. The electromagnetic field present in the plasma acts as a potential barrier for the incoming cosmic radiation, when the shock front passes in the vicinity of the Earth. As a consequence, the observed rate of the secondary particles (neutrons and muons etc. produced by the primary cosmic rays) in the atmosphere of the Earth registers a sudden drop, which is termed ''Forbush decrease'' [18]. The passage of the Earth through the shock front results in the sudden commencement of a geomagnetic storm. Several variants of the shock models involving ordered and/or turbulent magnetic fields have been proposed to explain the phenomenon of Fd [19].

The Fds are characterized by a rapid decrease ($\sim$ 5%–15%) in the intensities of the observed muon and neutron fluxes at the Earth with an onset time, ranging from several hours to about a day. This is followed by a relatively slower recovery time, ranging from about a week to several months. The magnitude of a Fd is defined as the fractional decrease in the intensity of the muon/neutron flux from its quiescent value. The magnitude of the Fds is observed to decrease with increasing rigidity. The Fds also display some correlation with the 11-year solar cycle. The occurrence of the Fds is generally accompanied by the observation of large anisotropies in the flux of the cosmic radiation [19]. The phenomenon responsible for a Fd evolves as it propagates farther into the heliosphere. This evolution results in a gradual increase in the onset and the recovery times with the heliocentric distance. There have been suggestions that the cosmic ray modulation with the 11-year solar cycle could be a result of the cumulative effects of the Fds occurring over a long period of time [20].

The ground-based NMs and space-borne detectors in general have a very poor angular resolution. Therefore, the information on the directional dependence of the Fds is usually obtained from the worldwide network of ground-based NMs located all over the Earth, with the help of appropriate modeling techniques [21,22]. However, due to the variation in the cutoff rigidity with the geomagnetic latitude of the site, various NMs respond differently to a given Fd event, thus making the interpretation of the observed data somewhat complicated and model dependent. However, a single monitor with a good angular resolution may be able to provide simultaneous information on the directional dependence of the observed Fd. In addition, the detectors located near the geomagnetic equator have rigidity cutoff, which varies rapidly with the arrival direction, thus permitting the measurement of the rigidity dependence of the detected Fd from a single instrument.

The arrival of the CME on 29 October 2003, $\sim$20 h after the start of the X17 class solar flare at 09:51 UTC on 28 October 2003, started the onset of a large Fd. As described later in Sec. V, new information on this Fd has been provided by the GRAPES-3 experiment. The magnitude of this Fd as measured by the GRAPES-3 experiment is $\sim$8% and a comparatively short onset time of $\sim$10 h and thereafter the recovery phase of the Fd commenced. The onset and recovery phases of this Fd display a rich time structure. The tracking feature of the muon telescope has shown a systematic time shift in the onset of the Fd on a

time scale of an hour. By exploiting the tracking feature of the muon telescope for analyzing the rigidity of the incoming particles, the rigidity dependence of the magnitude of the Fd has been estimated.

## II. GRAPES-3 EXPERIMENTAL SYSTEM

The GRAPES-3 experiment is located at Ooty (11.4° N latitude, 76.7° E longitude, and 2200 m altitude), a popular mountain resort town in southern India. The GRAPES-3 air shower experiment has been designed to have one of the most compact configurations of the conventional type arrays with a separation of only 8 m between the adjacent detectors which are deployed in a symmetric hexagonal geometry. A schematic layout of the GRAPES-3 array is shown in Fig. 1. The observations were started in early 2000 with 217 detectors, located within the inner 8 rings which are shown as filled circles in Fig. 1. Depending on the supply of the plastic scintillators which are being continuously fabricated in-house, additional detectors are being regularly added. Currently the experiment is being operated with over 320 detectors. The final goal is to install 15 rings with 721 detectors, covering a total distance of 120 m from the center of the array. The detectors yet to be installed are shown as open circles in Fig. 1 [23].

A very large area tracking muon telescope operating as part of the GRAPES-3 experiment [23,24] is an unique instrument used to search for the high energy protons emitted during the active phase of a solar flare. The muon telescope is capable of providing a high statistics, directional study of muons. The GRAPES-3 muon telescope has a total area of 560 $m^2$, consisting of 16 modules, each of which is 35 $m^2$ in area. These modules are located very close to each other as shown in Fig. 1. A cluster of four 35 $m^2$ area neighboring modules, located inside a common hall, constitutes one supermodule with a total area of 140 $m^2$. In Fig. 2, a picture of the four halls, each housing one supermodule of the tracking muon telescope, is shown. Some of the scintillator detectors of the GRAPES-3 air shower array (sealed inside the pyramid shaped housing) which have been placed on the roof and around these halls are also visible [23]. The energy threshold of the telescope is 1 GeV for the muons arriving along the vertical direction. The cutoff rigidity at Ooty is 17 GV in the vertical direction and varies from 12 to 42 GV across the field of view of the tracking muon telescope as shown later in Fig. 9.

The basic detector element of the muon telescope is a rugged proportional counter (PRC) made from a 600 cm long steel pipe with 2.3 mm wall thickness and a square cross-sectional area of $10 \times 10$ $cm^2$. A muon detector module with a sensitive area of 35 $m^2$ consists of a total of 232 PRCs arranged in four layers of 58 PRCs each, with alternate layers placed in orthogonal directions. Two successive layers of the PRCs are separated by a 15 cm thick reinforced cement concrete layer, consisting of 60 cm × 60 cm × 15 cm blocks. The four-layer PRC configuration of the muon modules permits us to have a two-dimensional reconstruction of the muon tracks in two vertical, orthogonal planes, namely, XZ and YZ planes, where the Z axis lies along the vertical direction. The vertical separation of the two layers of the PRCs in the same projection plane is ~50 cm, which allows the direction of the muon track to

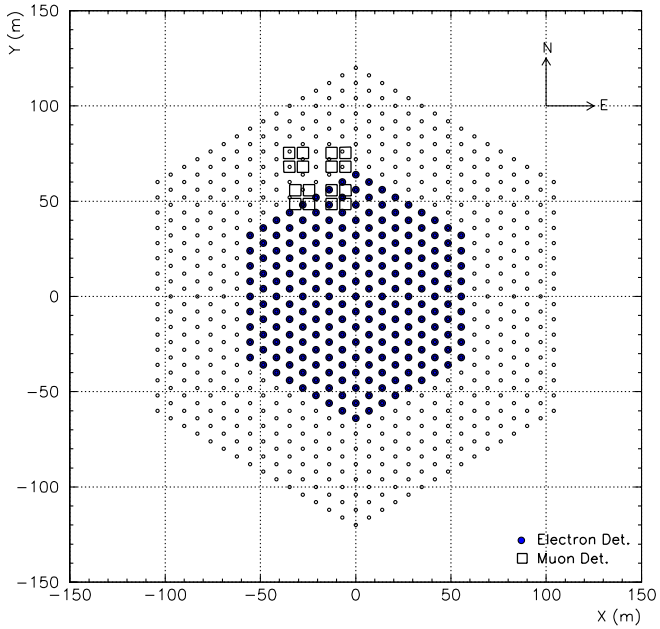


FIG. 1 (color online). A schematic layout for the 721 detector (open circles) GRAPES-3 shower array of which 217 detectors (filled circles) used at present are shown. Each of the 16 squares represents a 35 $m^2$ area muon tracking detector with $E_\mu \geq 1$ GeV.

FIG. 2 (color online). A view of the GRAPES-3 experiment showing the four halls housing the four supermodules of the muon detector. The scintillator detectors of the GRAPES-3 air shower array, placed on the roof and around the muon halls are also visible.

be measured to an accuracy of $\sim 6^\circ$ in each of the two projected planes.

In order to achieve an energy threshold of 1 GeV for the vertical muons, a total thickness $\sim 550$ g cm$^{-2}$ in the form of concrete blocks has been employed as the absorber. This has been done by placing a total of 15 layers of concrete blocks above layer 1, as is shown schematically in Fig. 3. A unique feature of the GRAPES-3 muon detector is the robust structure of the PRCs which has permitted it to support the huge load of a 2.4 m thick concrete absorber in a self-supporting manner. The concrete blocks have been arranged in the shape of an inverted pyramid to shield the PRCs, with a coverage of up to $45^\circ$ for the incident muons. The detectors have an energy threshold 1 ( sec$\theta$) GeV for the muons incident at a zenith angle of $\theta$. The cross section of a muon detector module is shown schematically in Fig. 3. As mentioned earlier, a cluster of four such modules separated by a horizontal distance of 130 cm at the base constitutes one supermodule. The GRAPES-3 muon detector contains a total of four supermodules [24].

Because of the sensitivity of the PRCs to low-energy $\gamma$ rays from the radioactivity present in the concrete absorber, individual PRCs display sizable counting rates of $\sim 200$ Hz. When an output is generated, if any one of the 58 signals is present, is termed an OR. A coincidence of the OR outputs from the four layers of a module is used to generate a 4-layer trigger. Despite the high counting rates of the individual PRCs due to the radioactivity that is present in the surrounding absorber, the 4-layer coincidence triggers are relatively free from this background and represent the passage of through going muons. The observed 4-layer muon counting rate of $\sim 3200$ Hz per module yields a total counting rate $\sim 3 \times 10^6$ min$^{-1}$ for all 16 modules. This large rate of muons permits even a small change of $\lesssim 0.1\%$ in the muon flux to be detected over a time scale of $\sim 5$ min after the application of appropriate corrections for the variation in the atmospheric pressure.

Unfortunately, during the period 28–29 October 2003, only three out of four supermodules were continuously operating. Therefore, in all subsequent discussions the data from only 12 working modules have been used. In Fig. 4, the percent variation in the 4-layer muon rate as recorded by one of the 12 working modules relative to the remaining 11 modules is shown for 28 October 2003. The horizontal axis in Fig. 4 represents the coordinated universal time (UTC) in hours for 28 October 2003. The percent variation observed in the muon rates is consistent with a statistical error of 0.04%, expected from the total muon counts ( $\sim 6 \times 10^6$) in the sample. Similar results have been obtained for the remaining modules. However, a limiting value of the precision of $\sim 0.016\%$ is obtained, in cases where the statistical error from the total muon count in the sample is significantly smaller than this value. We attribute this limiting precision (0.016%) to the overall stability of the detector system and to the irreducible systematic errors present in the data. This high level of precision permits a very detailed study of the cosmic ray intensity variation to be carried out. For example, the onset of the Forbush decrease on 29 October 2003 which started $\sim 20$ h after the start of an X17 class solar flare at 09:51 UTC on 28 October 2003 [25] has been studied in considerable detail with the GRAPES-3 instrument.

However, most of the detected muons are generated by $\gtrsim 20$ GeV galactic cosmic rays, which are of little interest to us here, except for the fact that they form a stable and dominant background to the variation in the muon flux produced by the solar flare. The statistical variations in the muon rate are relatively small in magnitude because of the large area of the GRAPES-3 muon telescope, where $\sim 3 \times 10^6$ muons are detected every minute from the hits recorded in the 3712 PRCs of the GRAPES-3 muon telescope [24]. The muon data is grouped online every 10 sec, into solid angle bins of $\sim 0.05$ sr, consistent with the angular resolution of the muon telescope as detailed below. However, despite the drastic reduction in the data generated due to this angular segmentation, we still record $\sim 9$ GB of data from the four supermodules every day.

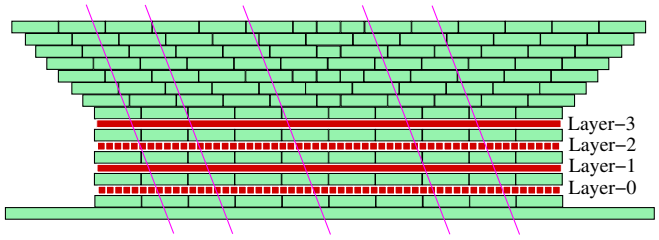


FIG. 3 (color online). A schematic display of the 4-layer tracking muon detector module with 58 PRCs per layer. The four layers of the PRCs labeled Layer-0, Layer-1, etc. are embedded in concrete blocks. Inclined lines represent a set of parallel muon tracks.

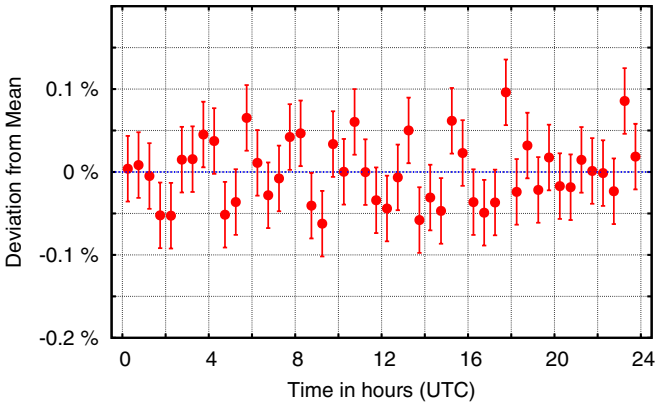


FIG. 4 (color online). The percent deviation in the 4-layer muon counting rate of one of the 35 m$^2$ area module relative to the mean rate of remaining 11 modules as a function of time, on 28 October 2003. The rates are taken for 30 min intervals.

## III. SOLAR PROTON EMISSION

The relativistic solar particles can provide a key to the understanding of the acceleration processes at work in the Sun. The global network of NMs has been used to detect relativistic neutrons produced in the atmosphere from the interactions of the high energy particles from the Sun, which were accelerated during the solar flare on 28 October 2003 around 11:10 UTC nearly 80 min after the detection of this flare in x rays. This solar flare had followed in the wake of the highly disturbed interplanetary conditions prevailing because of the earlier eruptions that had occurred in the Sun.

We have searched for the direct emission of protons at the time of this solar flare. However, during the period of interest as mentioned earlier, only three out of four supermodules were operating and therefore the total area of the muon detector was reduced to 420 $m^2$. In Fig. 5 the pressure-corrected GRAPES-3 data of 28 October 2003 for the muon rates summed over the three working supermodules is displayed. The variation in the rate of muons, with an amplitude of $\sim$1% due to the diurnal anisotropy is clearly visible. However, no statistically significant excess has been recorded in the time interval of 30 min after the start of the solar flare at 09:51 h UTC, indicated by the first arrow in Fig. 5 or after 11:10 h UTC, indicated by the second arrow when the global network of NMs started recording increase in the rate of neutrons.

The value of 30 min has been selected as the energetic (multi-GeV) protons are expected to arrive within 1–2 times the light travel time (8–16 min) from the Sun to the Earth as given in the model quoted above [3]. However, in the absence of the precise knowledge of the energy spectrum of solar protons at high energy and that of the interplanetary magnetic field, there is a considerable degree of uncertainty in the actual travel time of the energetic solar protons. The NM data showed the presence of the proton flux over an extended period of time. Thus an interval of 30 min is expected to provide a reasonable time window for the detection of any direct high energy protons from the solar flare. The exact choice of the time window is not a critical parameter because the upper limit on the proton flux as is described below, is not particularly sensitive to the duration of the time window selected.

To further investigate the possibility of emission of protons on time scales shorter than 30 min, the data has been analyzed for intervals of 1, 3, and 6 min for a limited time window from 09:00 to 13:00 h UTC and is shown in Fig. 6. The percent change in the total rate of muons, detected by the three working supermodules for the 1, 3, and 6 min intervals is shown in the top, middle, and bottom panels of Fig. 6, respectively. The arrow on the left in each panel indicates the start of the x-ray flare and the arrow on the right the start of a flux detected by NMs. However, no statistically significant excess is seen anywhere during the interval 9–13 h UTC. The systematic decrease in the muon rate, seen in Fig. 6, is due to the well-known diurnal anisotropy.

Since $>$1 GeV muons are secondaries produced by the primary protons of energy $\gtrsim$ 20 GeV in the atmosphere, these observations have been used to place a 99% C.L. upper limit of $1.4 \times 10^{-6}$ $cm^{-2}\,s^{-1}\,sr^{-1}$ on the wide-angle ( $\sim$ 2.5 sr) flux of solar protons. The tracking muon tele-

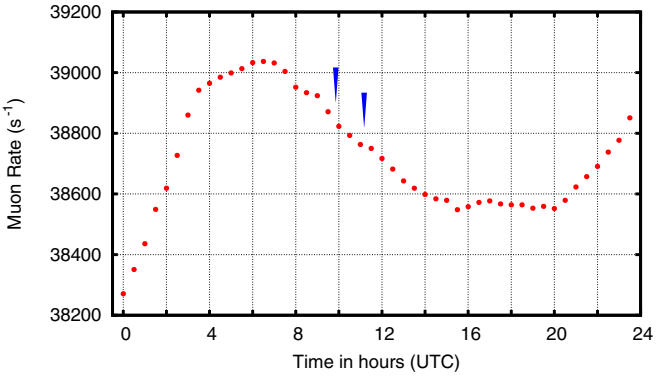


FIG. 5 (color online). The variation in the total muon rate for the three supermodules, for 28 October 2003 after atmospheric pressure correction. Start of the solar flare is indicated by the first arrow. The second arrow indicates the start of the prompt component detected by NMs.

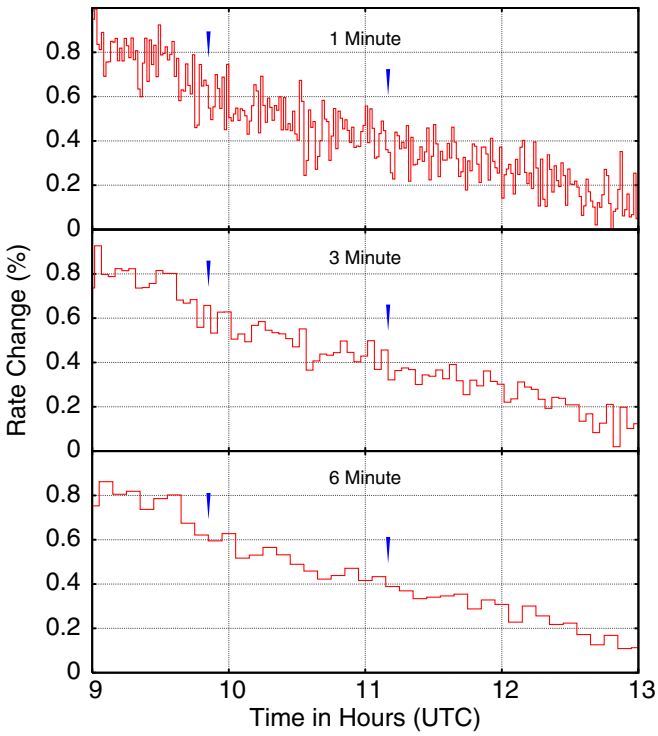


FIG. 6 (color online). The percent variation in the total muon rate for the three supermodules, for 28 October 2003 9–13 h UTC; (i) for 1 min interval (top panel), (ii) for 3 min (middle), and (iii) for 6 min (bottom). The left and right arrows in each panel indicate the start of the x-ray flare and that of the prompt component detected by NMs.

scope is being operated round the clock to search for direct protons during the solar flares which may occur in the future.

## IV. NARROW-ANGLE SOLAR PROTON EMISSION

It is well known that the solar protons of energies of tens of GeV, need not be observed from the direction of the Sun, due to their deflection in the interplanetary and geomagnetic fields. Therefore, it is possible to enhance the sensitivity of the muon detector by incorporating the measurement of the arrival direction of the muons. This novel feature has been incorporated into all four supermodules of the GRAPES-3 detector by recording the muon directions into 225 solid angle bins. This capability has been achieved after the installation of new, additional direction-sensitive trigger electronics and a separate data acquisition system for each of the four supermodules. As is shown in Fig. 7, for each PRC in the lower layer, the muon angle is determined and binned into 15 angular bins based on the specific PRC triggered in the upper layer from among the 15 PRCs, one directly above (central PRC) and 7 each on either side of the central PRC. This angular binning is carried out in each of the two orthogonal projections (XZ and YZ), thereby generating a two-dimensional $15 \times 15 = 225$ solid angle map of the muon directions. The contents of the 225 solid angle bins are recorded, once every 10 s, thus permitting a continuous monitoring of the directional flux of the muons in the sky.

Although the excess in the muon rate can be searched for in any of the 225 solid angle bins, it is expected that the flux of the solar protons from a flare would be spread over several bins. This directional spread could arise from a number of factors, namely, (a) the size of the bin is comparable to the angular resolution of the muon telescope, (b) the magnetic field in the solar flare and in the interplanetary regions, (c) the terrestrial magnetic field, and (d) the transverse momentum imparted in the atmospheric collisions. Therefore, for the purposes of the present study, the muons have been regrouped into $3 \times 3 = 9$ coarse solid angle bins, as shown schematically in Fig. 8. This regrouping of the data has been done by either combining a set of $3 \times 5$ or $5 \times 5$ solid angle bins. The exception being the vertical direction which combines $3 \times 3$ bins. This peculiar choice of binning is dictated by the fact that the muon flux is comparatively larger for the near central directions (N, E, W, S) as compared to the outer directions (NE, SE, NW, SW). This regrouping of the data results in a relatively similar solid angle coverage for the nine bins. Therefore, this rebinning also results in muon statistics for various bins which are not too dissimilar from each other.

The geomagnetic cutoff rigidity for the field of view (FOV) of the GRAPES-3 muon telescope varies significantly for the nine solid angle bins. In Fig. 9 the contours of constant geomagnetic cutoff rigidity in the FOV are superimposed over a schematic of the nine solid angle bins of muon arrival directions in two orthogonal projected planes. The geomagnetic cutoff rigidity varies from a low value of 12 GV in the West to 42 GV in the East direction within the FOV of the GRAPES-3 tracking muon telescope. The measurement of the direction of muons in GRAPES-3 experiment permits the effect of the rigidity on various solar phenomena to be systematically studied as described later in Sec. VI.

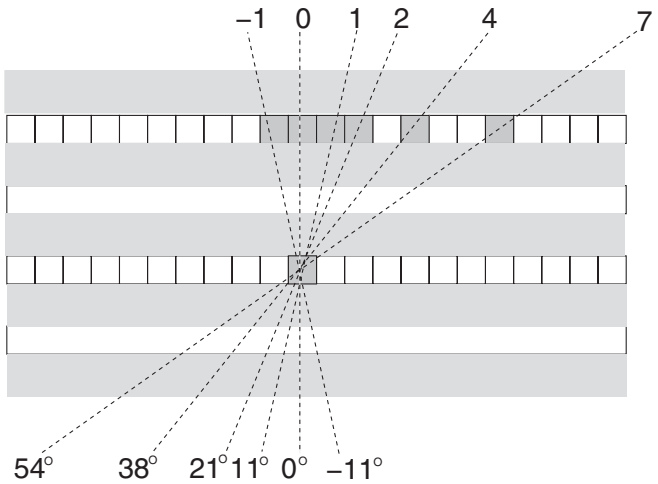


FIG. 7. A schematic view of muon arrival angle selection based on the PRC triggered in the lower and 15 PRCs directly above, in the upper layer. Triggered PRCs are shown as filled squares.

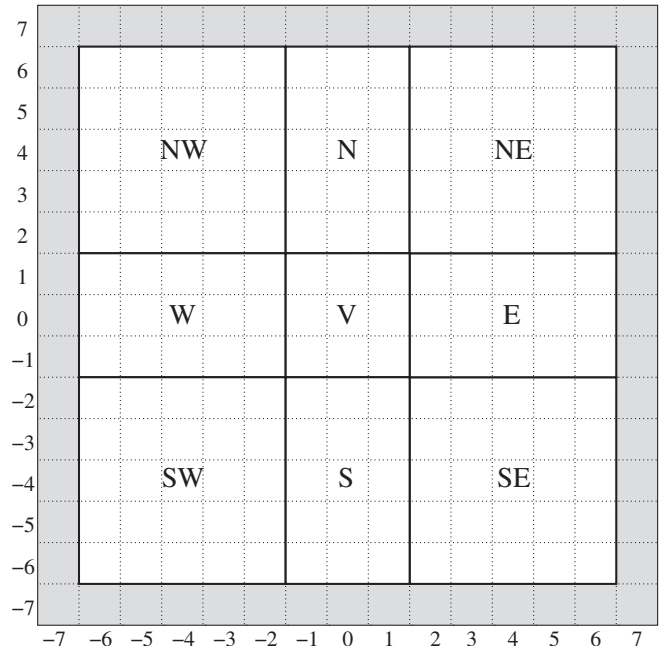


FIG. 8. A schematic of the nine groups of muon arrival directions which combine to form solid angle bins; $3 \times 3$ vertical bin V or four $3 \times 5$ central bins N, E, W, S or four $5 \times 5$ outer bins NE, SE, SW, NW.

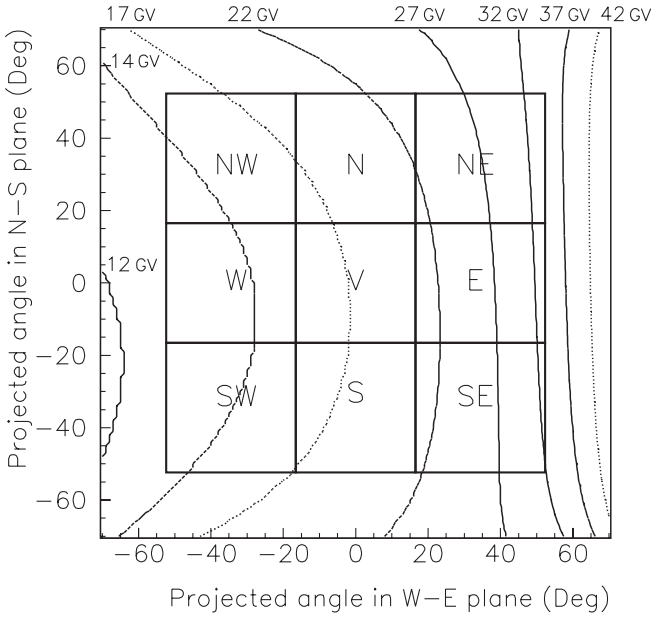


FIG. 9. A schematic of the nine solid angle bins of muon arrival directions. Also shown are contours of constant geomagnetic cutoff rigidity in the field of view. The cutoff rigidity varies from 12 to 42 GV in the FOV of GRAPES-3 muon telescope.

With the enhancement in the directional sensitivity, achieved through this angular segmentation, the fractional variation in the muon counting rate for time intervals of 6 min is shown in Fig. 10 for the nine solid angle bins. The diurnal anisotropy observed in the wide-angle data shown in Fig. 5 is also visible for all nine directions. However, the time of the maximum amplitude of the anisotropy seems to change with the arrival direction. For example, the maximum amplitude is reached earliest for the three East (NE, E, SE) directions, followed by the Center (N, V, S) and finally the West (NW, W, SW) directions. This time evolution is discussed, in greater detail later on, in Sec. V.

No statistically significant excess is seen, from any of the nine directions in the muon rate, during an interval of 30 min, after the start of the solar flare at 09:51 h UTC on 28 October 2003. A 99% C.L. upper limit of $4 \times 10^{-6}$ cm$^{-2}$ s$^{-1}$ sr$^{-1}$ on the narrow-angle ( $\sim 0.3$ sr) flux of the solar protons of $\gtrsim 20$ GeV from each of the nine angular regions has been placed. An analysis of this data on shorter time scales, similar to that of the wide-angle data, described earlier in Sec. III, also did not reveal any statistically significant excess on time scales of 1, 3, and 6 min for all nine directions.

The GRAPES-3 wide-angle upper limit along with those obtained for the solar flares of 29 September 1989 by the Baksan group [15] and of 14 July 2000 by the L3 group [17] are also shown in Fig. 11. A flux of neutron of $2 \times 10^{-4}$ cm$^{-2}$ s$^{-1}$ above 10 GeV claimed by the AGASA group [16] for the solar flare of 4 June 1991 is shown in Fig. 11. For a comparison, the flux of particles recorded using NMs during one of the largest flares recorded on 23 February 1956 and the one on 15 April 2001 are also shown in Fig. 11.

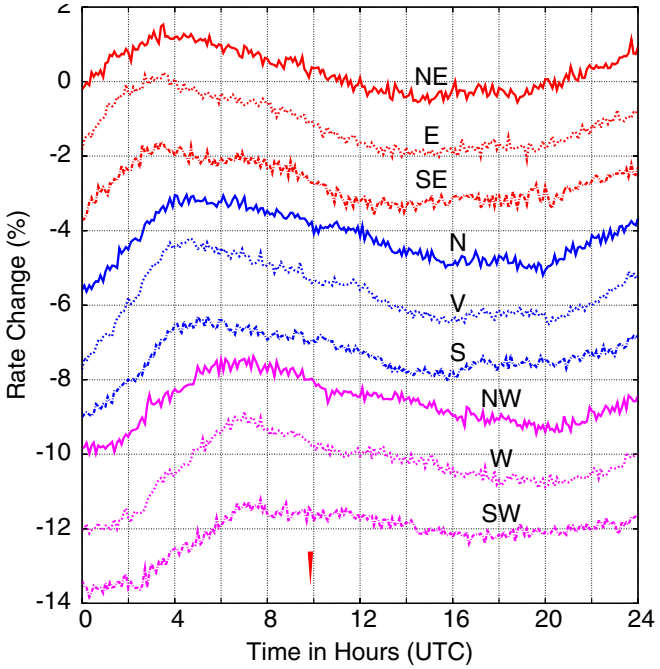


FIG. 10 (color online). The observed variation in the muon rate on 28 October 2003 for nine solid angle bins is shown, for 6 min intervals. Successive plots have been shifted down by 1.5% for clarity. The start of solar flare is indicated by the arrow.

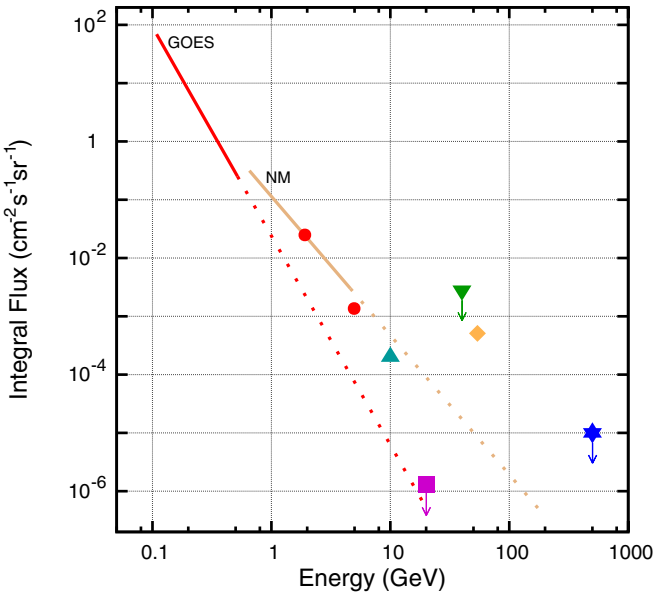


FIG. 11 (color online). Integral flux of protons with energy on 28 October 2003; (a) based on 100–600 MeV GOES-10/11 and sub-GeV balloon data, (b) worldwide NM data, (c) ■ $\gtrsim 20$ GeV GRAPES-3 upper limit, (d) ▲ >10 GeV AGASA flux on 4 June 1991, (e) ▼ >40 GeV L3 upper limit on 14 July 2000, (f) ★ >500 GeV Baksan upper limit on 29 September 1989, (g) ● NM data on 15 April 2001, (h) ◆ NM data on 23 February 1956.

The GOES-10/11 instruments had recorded a rapid increase in the flux of >100 MeV proton at ~11:30 h on 28 October 2003. The flux of proton at >100 MeV had increased by almost 2 orders of magnitude in the next 2 h and then started declining slowly 12 h later around 23:30 h UTC on 28 October 2003. The straight line at the top left of Fig. 11 represents a power law fit to the integral energy spectrum of the protons, in the energy range 100–600 MeV as measured by the GOES-10/11 satellites on 28 October 2003 [26]. The power law fit to the energy spectrum, extrapolated beyond observed GOES energies, is shown by a dotted line. The measurements made on the flux of sub-GeV protons on a balloon flight on the same day is also in excellent agreement with the GOES data [3]. The second straight line shown in Fig. 11 represents a power law fit to the integral energy spectrum of GeV protons based on the measurements of the worldwide network of NMs on 28 October 2003. The power law fit to the energy spectrum, extrapolated beyond observed NM energies, is shown by a dotted line.

In the absence of the NM data, the upper limit from the GRAPES-3 experiment would have been consistent with the extrapolation of the low-energy GOES data, as seen in Fig. 11. However, the NM data of 28 October 2003 displays an energy spectrum, which seems to significantly harden in the GeV energy range. However, this trend must reverse itself, and the energy spectrum beyond 5 GeV should either soften rapidly or there should be a cutoff in order to be consistent with the upper limit at 20 GeV derived from the GRAPES-3 data. However, in the absence of rapid softening of the energy spectrum or a cutoff, the extrapolation of the NM data is 2 orders of magnitude higher than the GRAPES-3 upper limit. The lower limit on an assumed power law spectral slope based on the NM and GRAPES-3 data is $\gamma \sim 5.3$. If the flux of 20 GeV protons were comparable to the positive flux values reported by the AGASA and other groups, the GRAPES-3 would have detected it as an increase $\gtrsim 5\%$ of the ambient cosmic ray flux. Such a large increase would be almost impossible to miss in the GRAPES-3 data.

Here note that the muons detected by the Baksan and the L3 groups were at energies which were significantly higher (1–2 orders of magnitude) as compared to the GRAPES-3 experiment. However, the energy threshold of solar cosmic rays responsible for the muons detected by the AGASA group was much closer to that of the GRAPES-3 experiment and, therefore, permitted a more meaningful comparison of their results. However, unlike the GRAPES-3 experiment, the absence of a tracking muon telescope in the AGASA experiment compelled that group to utilize their unshielded plastic scintillator detectors in the array, for the measurement of the muons produced in the atmosphere by the solar flare particles. Therefore, the AGASA group had to rely on the net increase in the counting rate of their scintillation detectors, which then was attributed to the muons produced by the solar flare particles. A clear cut identification of the muons and their arrival direction in a tracking muon telescope as in the case of the GRAPES-3 was not possible for the AGASA experiment.

Since the 4 June 1991 solar flare occurred near the east limb of the Sun, the protons originating there are expected to arrive at the Earth after a delay of ~1–2 h after the onset of the x-ray emission based on earlier flare observations [16]. However, the near coincident (within a few minutes) increase in the muon flux with the onset of the x-ray emission prompted the AGASA group to conclude that the parent particle of muons should be neutrons. The presence of the three muon detectors at altitudes of 2700 m (Mt. Norikura), 900 m (AGASA), and sea level (Nagoya) had permitted them to estimate the attenuation length of the neutrons in the atmosphere. The measured attenuation length turned out to be anomalously large at 200 $\mathrm{g\,cm^{-2}}$ as compared to the normal value ~100–120 $\mathrm{g\,cm^{-2}}$. The AGASA group also estimated that the spectral index of the power law describing the neutron flux was ~4–5. The flux of the solar neutrons for the 4 June 1991 flare was estimated to be $1\text{–}2 \times 10^{-4}$ $\mathrm{cm^{-2}\,s^{-1}}$ which is about 2 orders of magnitude larger than the 99% C.L. upper limit of $1.4 \times 10^{-6}$ $\mathrm{cm^{-2}\,s^{-1}\,sr^{-1}}$ on the wide-angle flux of the particles placed by GRAPES-3 for the 28 October 2003 flare. In addition, the tracking feature of GRAPES-3 muon telescope allowed us to place a slightly less stringent 99% C.L. upper limit of $4 \times 10^{-6}$ $\mathrm{cm^{-2}\,s^{-1}\,sr^{-1}}$ on the narrow-angle flux of solar flare particles, for which, in absence of tracking, there is no counterpart in the AGASA experiment.

Based on the past observations, the energy spectra of the particles accelerated in the solar flares display considerable complexity. It is reasonable to assume that the energy spectrum of the particles accelerated during a solar flare follow a power law. A compilation of the major solar flare events during the past 60 yr has shown that the spectral index of the assumed power law shows progressive steepening with increasing energy of protons, reaching a value of 3.5–4.0 at energies above 10 GeV [27]. However, it is very difficult to arrive at a definitive conclusion on the energy spectrum of the solar flare particles in view of the huge variation seen from flare to flare; based on the past claims, it is likely that the solar flares may accelerate protons to energies well above 100 GeV [12,15]. A lower limit on the spectral index of an assumed power law for the energy spectrum of the 28 October 2003 flare can be placed at $\gamma \sim 5.3$ based only on the worldwide NM and the GRAPES-3 data. However, in view of the rapidly changing spectral indices and/or cutoffs observed in the case of most of the solar flares, the actual value of the spectral index is likely to be significantly higher [27]. The narrow-angle upper limits on the flux of solar flare particles derived for the nine bins are very similar and for that reason a common value of $4 \times 10^{-6}$ $\mathrm{cm^{-2}\,s^{-1}\,sr^{-1}}$ has been quoted above.

## V. FORBUSH DECREASE ON 29 OCTOBER 2003

In addition to the acceleration of particles due to the energy released from the coronal loops, the solar flares are also associated with the coronal mass ejections which are blobs of plasma ejected during the flaring activity. An expanding CME-driven shock front accelerates ions at various helio-longitudes. Apart from the complex structure of a CME and its interaction with the heliospheric magnetic cavity, its effect on the structure of the geomagnetic field is also very important for various studies at the Earth. It is widely recognized that the CMEs and high-speed streams from the coronal holes have considerable influence on the propagation of the particles within the heliosphere. The interaction of these flows with the quiet solar wind creates regions of compressed heated plasma and shocks which are responsible for further acceleration and modulation of the particles incident over the atmosphere of the Earth. Detailed observations on the modulation of the cosmic rays, using NMs and muon telescopes, provide important information for modeling the propagation and acceleration of the solar energetic particles in the interplanetary medium. The short-term modulations such as Fds may be related, either directly to the material ejected from the Sun or to the transient interplanetary shocks generated by these ejections [19,20,28].

The capability to observe the directional muon flux, with the three working supermodules, provides a completely new view of the evolution of a Fd, which should help in modeling the propagation of the high energy particles in the interplanetary and in the near-Earth regions. This may be seen from the detailed information available on the Fd, observed on 29 October 2003 from the nine solid angle bins, each with a solid angle coverage of $\sim$0.3 sr as displayed in Fig. 8. The observed muon rate for time intervals of 6 min for one of the nine bins, namely, "V," after applying appropriate corrections for the variation in the atmospheric pressure as a function of time in hours UTC on 29 October 2003, is shown in Fig. 12. The rapid onset of the Forbush decrease starting around 7 h and lasting until 18 h UTC is clearly visible. Also shown in Fig. 12 is a dot next to the legend $1\sigma$ whose diameter represents the size of a $1\sigma$ error bar. Therefore, the rich structure in the muon rate seen during the onset of Fd is to be regarded as real, and it indicates the rapid variation in the evolution of the Fd on a time scale of minutes. It has been pointed out that a "two-step" structure observed in several Fds is caused by the ejecta and the shock effects of the CME [28]. Therefore, any model proposed to account for the particle acceleration and propagation through the interplanetary space during a solar flare should also be able to explain this rich time structure during the onset phase of the Fd.

The Tibet neutron monitor (NM) operated by the Japan-China collaboration is located at Yangbajing in Tibet (30.1° N latitude, 90.5° E longitude and 4300 m altitude) [29]. For a comparison of the GRAPES-3 muon data with the neutron data, the hourly rate of change of the neutron flux for the Tibet NM [30] is shown in Fig. 13 as a function of time in hours UTC on 29 October 2003. The geomagnetic cutoff rigidity of 14 GV in the vertical direction at Tibet is only slightly lower than 17 GV at Ooty. The proximity of the longitudes of Ooty and Yangbajing in Tibet (only 13.8° apart) implies that the same region of the sky is observed at these two locations almost concurrently. The onset of the Fd is clearly visible in Fig. 13 around the same time as in GRAPES-3 muon data shown in Fig. 12. The change in the neutron count rate has been calculated after normalizing it to the value observed at 00:00 h UTC on 29 October 2003. The magnitude of the

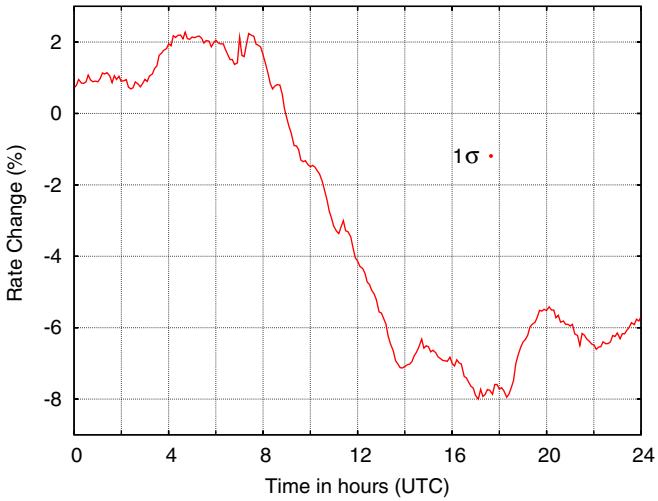


FIG. 12 (color online). The observed variation in the muon rate on 29 October 2003 from the vertical solid angle bin "V." Muon rates shown are for 6 min intervals. The diameter of the small dot to the right of legend $1\sigma$ equals 1 sigma statistical error in data.

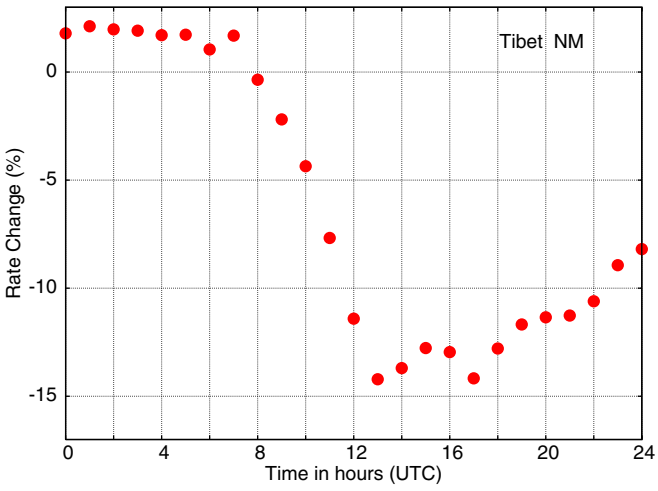


FIG. 13 (color online). The hourly variation in the observed neutron rate on 29 October 2003 for the Tibet neutron monitor. The change in rate is normalized, relative to the rate at 0 h UTC.

Fd is ~15% as compared to ~8% seen in GRAPES-3 muon data. The profile of the onset of the Fd is measured with much greater precision in the GRAPES-3 muon data, due to a higher count rate and shorter sampling interval. Therefore, the rich time structure seen in Fig. 12 is far less conspicuous in the NM data shown in Fig. 13. However, the overall profile of the Fd appears to be rather similar in both cases with a double valley structure near the bottom.

The observed muon rates for time intervals of 6 min for the nine bins, after applying the appropriate corrections for the variation of the atmospheric pressure, are shown in Fig. 14. Note that there is a systematic variation at the time, when a specific feature in the muon rate appears in a given solid angle bin. To highlight this aspect, the data in Fig. 14 are displayed after grouping them in three separate sets labeled "East," "Center," and "West," respectively. The east set contains the data from the three eastern solid angle bins, namely, NE, E, and SE. Similarly the center set contains the data from solid angle bins N, V, S, and finally the west set contains data from the solid angle bins NW, W, SW. For clarity, data shown in Fig. 14 for center and west sets have been shifted downwards by 4% and 8% relative with respect to the east set. The three arrows in Fig. 14 point to the time when the Fd reaches its minimum value for each of the three sets.

To get a more quantitative comparison of the profiles of the Fd as a function of muon arrival direction, we have carried out a systematic correlation study between the data from a pair of solid angle bins. For this purpose the paired data is classified into three categories, namely, (1) where the two solid angle bins in the pair belong to the same set (a total of 9 pairs), (2) where the solid angle bins belong to the adjacent sets (a total of 18 pairs), and (3) where the solid angle bins belong to the extreme sets, namely, one each from east and west sets (a total of 9 pairs). The correlation coefficient $C_{i,j}(s)$ for the paired data of two solid angle bins $i$ and $j$ is calculated as a function of the shift in time "$s$" as shown below,

$$C_{i,j}(s) = \Sigma R_i(t) R_j(t+s) / (\Sigma R_i(t)^2 \Sigma R_j(t+s)^2)^{0.5}, \quad (1)$$

where $R_i$ is the percent change in muon rate observed for solid angle bin $i$, and $t$ runs over the period 7–19 h UTC on 29 October 2003 which coincides with the onset of the Fd, and the time-shift "$s$" is varied from $-4$ to $+4$ h in steps of 0.1 h. The paired data for $s = 0$ shows a very high degree of correlation of $(99.7 \pm 0.2)\%$, $(98.8 \pm 0.2)\%$, and $(96.3 \pm 0.3)\%$ for the categories $-1$, $-2$, and $-3$, respectively. As expected the correlation coefficient gradually decreases with the increasing angular separation in the east-west direction. However, there is no such prominent effect in the north-south direction. In Fig. 15 a plot of the correlation coefficient as a function of time-shift $s$ is shown for one pair, from each of the three categories. The correlation coefficient shows a maximum at a time shift of zero, 0.6 and 1.3 h, respectively, for the three categories.

The sensitivity of the GRAPES-3 muon data is highlighted by the fact that the correlation coefficient for category-2 data for the pair "N" and "NE" systematically increases from 98.8% to 99.6% as the time shift was varied from 0 to 0.6 h in the correct direction as seen from Fig. 15. Although the increase of 0.8% in the magnitude of the correlation coefficient is modest, given the small value of

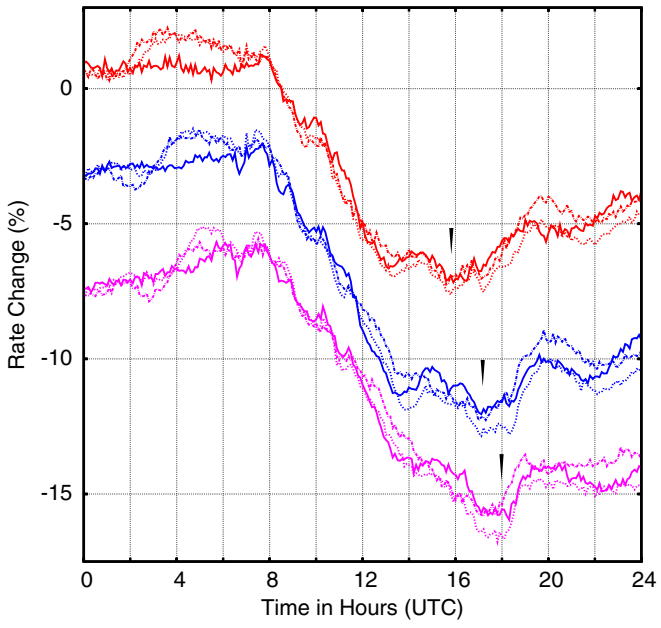


FIG. 14 (color online). The observed variation in the muon rate on 29 October 2003 from the nine angular bins grouped into three sets, namely, east (NE, E, SE), center (N, V, S), and west (NW, W, SW). Muon rates shown are for 6 min intervals. Successive sets have been shifted downwards by 4% for clarity. Each pointer represents the time of the Fd minimum for the 3 sets, respectively.

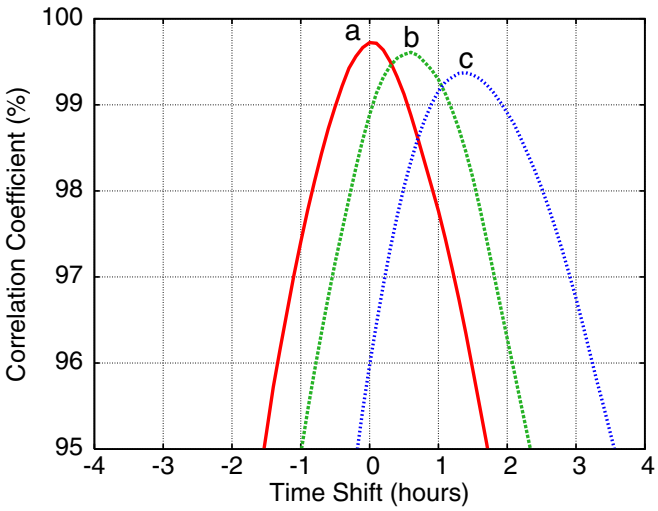


FIG. 15 (color online). Observed variation in the correlation coefficient with time shift (hours) for pairs of angular bins; (a) - category-1, W-SW, (b) category-2, N-NE, (c) category-3, E-W for the data of 29 October 2003.

statistical error ( $\sim 0.1\%$) in the GRAPES-3 data, even this modest increase is significant. But a time shift of 0.6 h in the opposite direction decreases the correlation coefficient to a comparatively lower value of 97%. The observed increase in the magnitude of the correlation coefficient of 3.1% is much larger for the category-3 data, for the pair ''E'' and ''W'' from 96.3% to 99.4% as the time shift is increased from 0 to 1.3 h in the correct direction as seen from Fig. 15. However, a time shift of 1.3 h in the opposite direction decreases the correlation coefficient to a value well below 90%.

The angular resolution of the muon telescope is $\sim 6°$ in each of the two vertical projection planes and the solid angle covered by each of the nine bins is $\sim 0.3$ sr. Therefore, the effective hour angle spanned by each bin is $\sim 25°$. Thus it should take about 1.7 h for a source in the sky to transit across the field of view of each of the nine solid angle bins. Therefore, purely from the hour angle arguments, it is expected that a Fd or any other phenomenon induced by the Sun, which produces a stable anisotropy should exhibit a time lag $\sim 1.7$ h for the category-2 and $\sim 3.3$ h for the category-3 data.

To test this ''hour angle'' hypothesis we have carried out an identical investigation of the correlation in the data of 27 October 2003. This day was selected as it was 1 day prior to the occurrence of the solar flare. The correlation coefficient is calculated for 36 pairs of solid angle bins on 27 October 2003, over a duration of 12 h which includes the diurnal anisotropy, using Eq. (1). This was done in exactly the same manner as for the data of 29 October 2003. In Fig. 16 a plot of the correlation coefficient as a function of the time-shift $s$ using Eq. (1) is shown for the three pairs, one each from the three categories. The three pairs selected are W-SW, N-NE, and E-W which are identical to the pairs used for the data of 29 October 2003 as shown in Fig. 15. The data for $s = 0$ still shows a sizable degree of correlation; (i) $(96.4 \pm 1.7)\%$ for the 9 pairs of the category-1, (ii) $(91.0 \pm 2.9)\%$ for 18 pairs of the category-2, and (iii) $(74.5 \pm 5.9)\%$ for the 9 pairs of category-3, respectively.

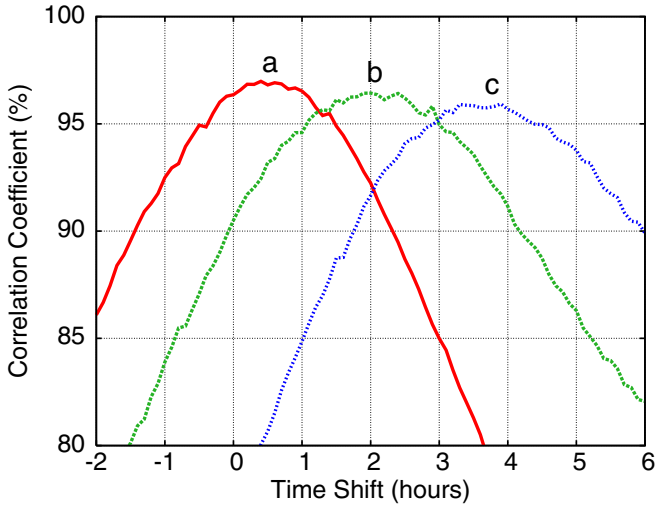


FIG. 16 (color online). Observed variation in the correlation coefficient with time shift (hours) for pairs of angular bins; (a) - category-1, W-SW, (b) category-2, N-NE, (c) category-3, E-W for the data of 27 October 2003, 1 day before the solar flare.

The correlation coefficient marginally increases from 96.4% to 96.8% for a time shift of 0.32 h with a dispersion of 0.28 h for the category-1 data. The correlation coefficient increases from 91.0% to 97.0% for a time shift of 1.92 h with a dispersion of 0.31 h for the category-2 data and from 74.5% to 95.3% for a time shift of 3.86 h with a dispersion of 0.21 h for the category-3 data. Therefore, a net time shift of $(1.6 \pm 0.4)$ h is observed between the category-1 and category-2 data which is very similar to the expected value of 1.7 h based on the hour angle calculations for the GRAPES-3 FOV. Similarly, the net time shift of $(3.5 \pm 0.4)$ h is observed between the category-1 and category-3 data, which is also very similar to the expected value of 3.3 h based on hour angle calculation for the GRAPES-3 FOV as seen in Fig. 16.

To summarize, the correlation study has shown a time offset of 0.6 and 1.3 h for categories-2 and -3 data, respectively, relative to the category-1 data during Fd of 29 October 2003. This is in stark contrast to a time offset of 1.6 and 3.5 h for the categories-2 and -3, respectively, relative to the category-1 data on 27 October 2003. As was already explained, the 27 October 2003 values are in agreement with the expectations based on the hour angle of the FOV of GRAPES-3 tracking muon telescope. Clearly, a rapid time evolution in the onset of the Fd on a time scale of $\sim 1$ h across a field of view of $\sim 25°$ is required to explain this reduction in the time offset from 1.7 to 0.6 h and from 3.3 to 1.3 h for the category-2 and category-3 data, respectively. The physical interpretation of the observed time evolution would require a detailed phenomenological modeling of the passage of the shock front produced by the CME and the effects on the cosmic ray intensity around the Earth.

## VI. RIGIDITY DEPENDENCE OF THE MAGNITUDE OF THE FORBUSH DECREASE OF 29 OCTOBER 2003

As shown in Fig. 9, the geomagnetic cutoff rigidity for the nine solid angle bins in the field of view of the GRAPES-3 tracking muon telescope varies from 12 GV to 42 GV. This fact combined with the high quality GRAPES-3 muon data, makes it possible to study the rigidity dependence of the magnitude of the Forbush decrease observed on 29 October 2003. The mean geomagnetic cutoff rigidity for the nine solid angle bins varies from 14.3 GV in west to 24.0 GV in the east direction. The muon rates averaged over 6 min successive intervals for the nine solid angle bins are used to estimate the magnitude of the Fd in each direction. In Fig. 17(a) the magnitude of the

Fd is shown, as a function of the geomagnetic cutoff rigidity for the nine bins. A clear inverse correlation between the geomagnetic cutoff rigidity and the magnitude of Fd can be noticed, because the magnitude of the Fd decreases as the cutoff rigidity increases. A change of 1.6% in the magnitude of the Fd is seen in going from 14.3 to 24 GV. However, another interesting feature of this variation is the setwise clustering of the values of the Fd magnitudes into groups of three bins (the three sets are described in Sec. V). The three east bins labeled NE, E, SE and represented by filled circles in Fig. 17(a) form a cluster. But the middle bin "E" shows a sizable departure in its magnitude ( $\sim 0.4\%$) as compared to the two outer bins NE and SE. Similarly the three "center" bins labeled N, V, and S and represented by filled triangles also show clustering with bin V separated by $\sim 0.5\%$ from the other two bins N and S. The displacement of bin W in the west set, represented by filled squares, is the largest $\sim 0.8\%$ with respect to the remaining two bins, namely, NW and SW.

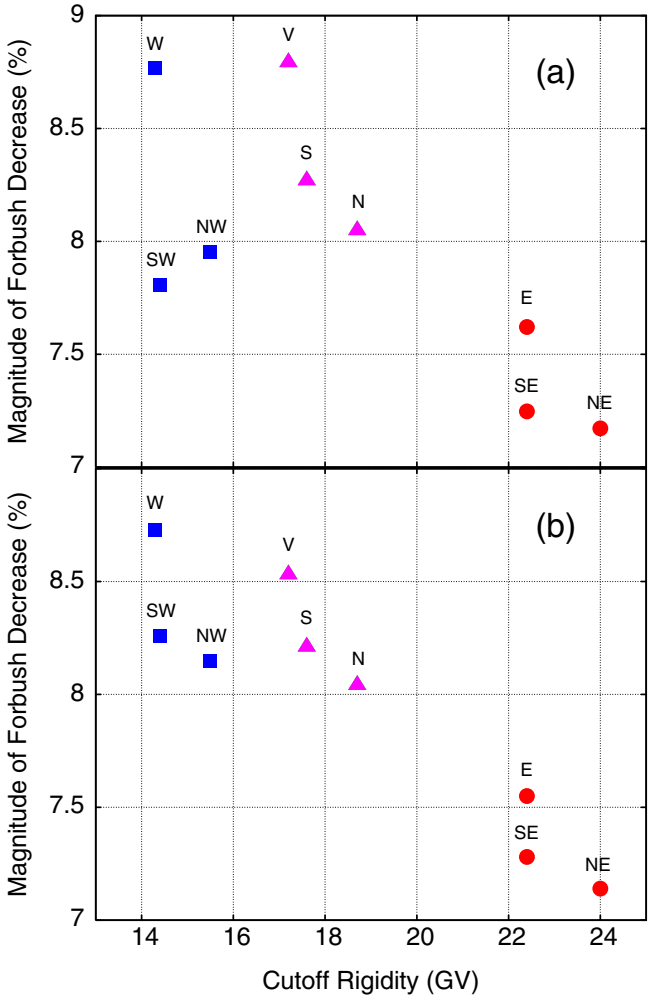


FIG. 17 (color online). (a) Observed variation in the magnitude of Forbush decrease (%); (b) simulations for the magnitude of Forbush decrease (%). Both as a function of geomagnetic cutoff rigidity (GV) for the three sets of nine solid angle bins, namely, (i) NE, E, SE (filled circles), (ii) N, V, S (filled triangles), (iii) NW, W, SW (filled squares). The middle bins (E, V, W) display sizable deviations $\sim 0.5\%$ from the remaining two bins. Simulations are for a rigidity dependence of Fd magnitude $= 12.8\% \times (r/30)^{-0.53}$.

The inverse correlation between the magnitude of the Fd and the geomagnetic cutoff rigidity is an established feature of the phenomenon of Fd, and it can be readily understood on the basis of the rigidity spectrum of the modulation of the cosmic rays. The rigidity dependence of the magnitude of the Fds have been measured by a number of groups primarily using NMs. The rigidity dependence can be reasonably approximated by a power law of the type $K \times r^{-\gamma}$ where $r$ is the rigidity in GV and the measured spectral index $\gamma$ ranges from 0.4 to 1.2 [28].

Although the observed displacement of the middle bin relative to the remaining two bins in each set is rather small ( $\sim 0.5\%$), given the small value of the statistical error in our measurements this effect becomes significant. Note that the middle bins (E, V, and W) in the respective sets of solid angle bins point to a direction, closest to the local vertical direction. Therefore, not surprisingly, these three bins record a larger flux of muons due to a lower threshold energy, caused by a relatively smaller angle of incidence. In order to determine the dependence of the magnitude "$A(r)$" of the Fd (in %) in a given bin, Monte Carlo simulations have been carried out with an assumed rigidity dependence described by the following power law:

$$A(r) = K(\%) \times (r/30)^{-\gamma} \qquad (2)$$

where $r$ is the rigidity in GV. In simulations effects of the instrumentation such as the rigidity cutoff, solid angle of acceptance, angle of incidence, etc. are included to compute the expected magnitude of the Fd, for the nine solid angle bins. A chi-square minimization method yielded the following values for the parameters of the power law fit: $K = (12.8 \pm 0.3)\%$ and $\gamma = 0.53 \pm 0.04$. This Monte Carlo simulation gave a rms spread of 0.19% in the magnitudes of observed and simulated data. A rms value of 0.19% between observed and simulated data sets, although larger than the intrinsic statistical error in the observed data of $\sim 0.1\%$, the agreement between the observations and the simulations is considered satisfactory in view of the numerous simplifications made in carrying out the Monte Carlo simulations.

The simulated magnitudes of the Fd for the nine solid angle bins are shown in Fig. 17(b). The simulated data reproduces the pattern of Fd magnitudes which is very similar to that of the observed data. The close agreement between Monte Carlo simulations and observations indicates that the major features of the data have been accounted for in terms of known effects such as the angle of incidence, energy threshold, etc. The value of the spectral index $\gamma = 0.53 \pm 0.04$ of the rigidity dependence of the magnitude $A(r)$ of the Fd is in agreement with the other measurements (0.4–1.2) as mentioned earlier [28]. Present

observations also demonstrate the ability of the GRAPES-3 muon telescope to make precision measurements on the solar phenomenon such as the Forbush decrease, including its rigidity dependence and anisotropy in real time.

## VII. SUMMARY

In summary, the salient features of the tracking muon telescope of the GRAPES-3 experiment at Ooty have been described in relation to the search for the direct emission of protons of $\gtrsim 20$ GeV in association with the solar flare of 28 October 2003. A 99% C.L. upper limit on the wide-angle flux of the solar protons is placed at $1.4 \times 10^{-6}$ cm$^{-2}$ s$^{-1}$ sr$^{-1}$. This upper limit is significantly lower than the limits and/or fluxes reported by the other experiments at comparable energies. The tracking feature built into the GRAPES-3 muon telescope has been exploited to carry out a narrow solid angle search of the direct protons. The negative result obtained has been used to place a 99% C.L. upper limit of $4 \times 10^{-6}$ cm$^{-2}$ s$^{-1}$ sr$^{-1}$. The significance of this novel feature of the GRAPES-3 muon telescope has been discussed in relation to the observations pertaining to the propagation of the solar flare particles in the interplanetary medium near the Earth. New information on the time evolution during the onset of the Forbush decrease of 29 October 2003, on a time scale of an hour, is provided. Rigidity dependence of the magnitude of the Fd, over a relatively narrow range of geomagnetic cutoff rigidity (14.3–24.0 GV) has been derived using the data from the tracking muon telescope. The estimated value of the spectral slope $\gamma = 0.53 \pm 0.04$ is in agreement with the earlier measurements which range from 0.4 to 1.2.

## ACKNOWLEDGMENTS

We thank D. B. Arjunan, K. Manjunath, B. Rajesh, and C. Ravindran for their help in the testing, installation, and operation of the proportional counters and the associated electronic modules. The administrative services of V. Viswanathan during all phases of the experiment are gratefully acknowledged. It is a pleasure to thank A. A. Basha, G. P. Francis, I. M. Haroon, V. Jeyakumar, and K. Ramadass for their help in the fabrication, assembly, and the installation of various mechanical components and detectors. The Japanese members of the GRAPES-3 Collaboration acknowledge the partial financial support from the Ministry of Education and Science of the Government of Japan for the GRAPES-3 experiment. The GRAPES-3 Collaboration also thanks N. K. Mondal and his colleagues in the TIFR-OCU Proton Decay Collaboration for the loan of the proportional counters which have been used in the muon detector. Finally, we thank the two anonymous referees whose critical comments led to a significantly improved presentation.

[1] See Space Weather web site on solar activity at www.spacew.com/astroalert.html.
[2] J. W. Bieber, Geophys. Res. Lett. **32**, L03S02 (2005).
[3] L. I. Miroshnichenko *et al.*, J. Geophys. Res. **110**, A09S08 (2005).
[4] See the ESA web site on SOHO results at www.esa.int/esaCP/SEMY3X7O0MD_index_0.html.
[5] K. Watanabe *et al.*, Astrophys. J. **636**, 1135 (2006).
[6] Z. Svestka, Space Sci. Rev. **95**, 135 (2001).
[7] J. A. Miller, Space Sci. Rev. **86**, 79 (1998).
[8] D. V. Reames *et al.*, Astrophys. J. Suppl. Ser. **90**, 649 (1994); D. V. Reames, Astrophys. J. **540**, L111 (2000); D. V. Reames and C. K. Ng, Astrophys. J. **610**, 510 (2004).
[9] B. Wibberenz *et al.*, Space Sci. Rev. **83**, 309 (1998); L. A. Fisk and N. A. Schwadron Space Sci. Rev. **97**, 21 (2001); Y. E. Litvinenko, Sol. Phys. **205**, 341 (2002); **216**, 189 (2003).
[10] N. Mandzhavidze and R. Ramaty, Nucl. Phys. B, Proc. Suppl. **33**, 141 (1993).
[11] S. W. Kahler *et al.*, Astrophys. J. **562**, 558 (2001).
[12] L. I. Miroshnichenko *et al.*, Space Sci. Rev. **91**, 615 (2000).
[13] M. J. Aschwanden, Space Sci. Rev. **101**, 1 (2002); P. Charbonneau *et al.*, Sol. Phys. **203**, 321 (2001).
[14] ACE Mission, Space Sci. Rev. **86**, 1 (1998).
[15] S. N. Karpov *et al.*, *Proceedings of 25th International Cosmic Ray Conference, Durban*, edited by M. S. Potgieter *et al.* (Potchefstroomse Universiteit, South Africa, 1997), Vol. 1, p. 205; Nuovo Cimento C **21**, 551 (1998).
[16] N. Chiba *et al.*, Astropart. Phys. **1**, 27 (1992).
[17] Y. Ma *et al.*, *Proceedings of 28th International Cosmic Ray Conference, Tsukuba*, (Universal Academy Press, Tokyo, 2003), Vol. 6, p. 3393; .
[18] S. E. Forbush, Phys. Rev. **54**, 975 (1938).
[19] J. A. Lockwood, Space Sci. Rev. **12**, 658 (1971).
[20] D. Venkatesan and Badruddin, Space Sci. Rev. **52**, 121 (1990).
[21] M. A. Shea and D. F. Smart, Space Sci. Rev. **32**, 251 (1982).
[22] L. J. Cramp *et al.*, J. Geophys. Res. **102**, 24 237 (1997).
[23] S. K. Gupta *et al.*, Nucl. Instrum. Methods Phys. Res., Sect. A **540**, 311 (2005).
[24] Y. Hayashi *et al.*, Nucl. Instrum. Methods Phys. Res., Sect. A **545**, 643 (2005).
[25] F. Spurny, K. Kudela, and T. Dachev, Space Weather **2**, S05001 (2004).
[26] See the NOAA web site on GOES satellite data at www.sec.noaa.gov/ftpdir/indices/old_indices.
[27] L. I. Miroshnichenko, *Proceedings of 28th International*

*Cosmic Ray Conference, Tsukuba*, T. Kajita *et al.* (Universal Academy Press, Tokyo, 2003), Vol. 6, p. 3321.
[28] H. V. Cane, Space Sci. Rev. **93**, 55 (2000).
[29] H. Miyasaka *et al.*, *Proceedings of 28th International Cosmic Ray Conference, Tsukuba*, (Universal Academy Press, Tokyo, 2003), Vol. 6, p. 3609.
[30] See Ibaraki University web site on neutron monitor data at www.env.sci.ibaraki.ac.jp/ftp/pub/WDCCR/STATIONS/tibet.